Searching for Conical Intersections of Potential Energy Surfaces with the ONIOM Method: Application to Previtamin D

Michael J. Bearpark,*,† Susan M. Larkin,† and Thom Vreven‡

Department of Chemistry, Imperial College London, South Kensington Campus, London SW7 2AZ, United Kingdom, and Gaussian, Incorporated, 340 Quinnipiac Street, Building 40, Wallingford, Connecticut 06492

Received: March 13, 2008; Revised Manuscript Received: May 13, 2008

We demonstrate that the ONIOM method can be used to optimize a conical intersection between the ground and first excited-state potential energy surfaces of previtamin D (precalciferol), with excitation localized in a small part of the molecule: the hexatriene chromophore. These calculations were up to 100 times faster with little loss of accuracy compared to a full non-ONIOM Target calculation. The most accurate ONIOM method combination was CASSCF/4-31G//ROHF/STO-3G(Triplet): in comparison to the Target (CASSCF/4-31G), bond lengths and angles in the hexatriene model region were calculated to within 0.02 Å and 0.7°, respectively, and the energy difference between the conical intersection and nearest associated S_1 minimum to within 0.5 kcal·mol^{-1}. All of the low-level methods selected produced accurate geometries, including the UFF molecular mechanics and AM1 semiempirical methods, suggesting a cheap and efficient way of initially optimizing conical intersections geometries. Furthermore, ONIOM allows for an assessment of the localization of excited states, providing some fundamental insight into the physical processes involved.

Introduction

Conical intersections are important in photochemical reactions since they permit rapid radiationless decay from excited electronic states.[1] As potential gateways for photochemical reactions, they are analogous to transition states for thermal reactions;[2] hence, we are interested in their structure and energetic accessibility to rationalize the formation (or lack) of any ground-state products.

We have recently reviewed[3] several different hybrid computational methods for calculating relaxation paths on the excited-state potential energy surfaces of large molecules. (Comparable applications to biological systems are reviewed—from a different perspective—in ref 4.) Here, we present the first systematic study of the ONIOM[5–11] hybrid method for locating conical intersections, at which nonadiabatic decay can take place.

ONIOM is a method that allows different *regions* of a chemical system to be defined, which are each treated with a different level of theory. The chemical process being investigated can therefore be treated at an appropriate high-accuracy computational level, while the remainder of the system (the "spectator" or low-level region) can be treated only with a lower level of theory. In this way, no computational time is "wasted" on parts of the system that do not need it.

The ONIOM energy is obtained through an extrapolation:

$$E^{\mathrm{ONIOM}} = E^{\mathrm{high}}_{\mathrm{model}} + E^{\mathrm{low}}_{\mathrm{real}} - E^{\mathrm{low}}_{\mathrm{model}} \qquad (1)$$

The *model* is a (sub)system based on a small fragment of the full *real* system/molecule, as shown for previtamin D in Figure 1. Here, the chemical process being studied—electronic excitation—will be localized in the model system. The *high*-level method is the more accurate quantum mechanical (QM) level of theory (CASSCF here), whereas the *low*-level method can be cheaper (e.g., HF, AM1, or UFF). ONIOM is an attempt to reproduce a calculation at the high level of theory for the real system, a calculation we define as the *Target* (and which we generally want to avoid carrying out, because of the computational cost). The absolute energy E^{ONIOM} (eq 1) differs (unless the high and low levels of theory are the same) from the absolute Target energy $E^{\mathrm{high}}_{\mathrm{real}}$. However, energy *differences* between two points on a potential energy surface (or between two potential energy surfaces at a particular geometry) will be reproduced

$$\Delta E^{\mathrm{Target}} = \Delta E^{\mathrm{high}}_{\mathrm{real}} \approx \Delta E^{\mathrm{ONIOM}} \qquad (2)$$

provided that the effects of changing partition size between regions, given by

$$E^{\mathrm{low}}_{\mathrm{real}} - E^{\mathrm{low}}_{\mathrm{model}} \qquad (3a)$$

and level of theory, given by

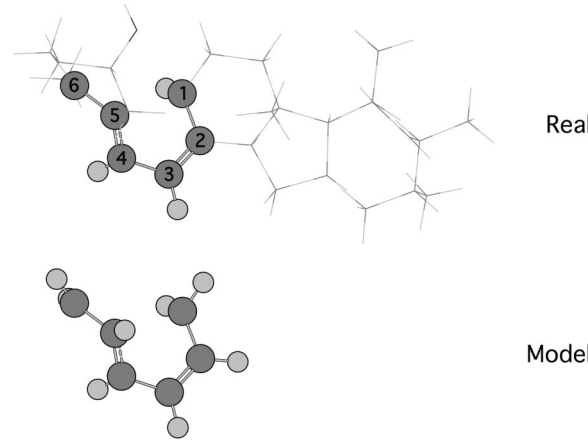

Figure 1. Previtamin D, showing the model (C_6H_8, ball-and-bond, bottom) and real ($C_{28}H_{44}O$, top) systems used in our ONIOM calculations. For the real system, atoms that belong to the high-level region are shown in ball-and-bond, and those that are in the low-level region are shown in wireframe.

* Corresponding author.
† Imperial College London.
‡ Gaussian, Incorporated.

10.1021/jp802204w CCC: $40.75 © 2008 American Chemical Society
Published on Web 07/17/2008

$$E^{\text{high}}_{\text{model}} - E^{\text{low}}_{\text{model}} \quad (3b)$$

are separable.

The ONIOM method adds the substituent effect to the high-level model calculation, saving computational time and resources by limiting (expensive and slow) accurate calculations to a small molecule fragment (e.g., Figure 1) where they are essential. The surroundings can be described by much cheaper and faster computational methods, which may give poor results on their own, yet have a beneficial effect on the model fragment calculation.[3]

ONIOM is a general hybrid method, since the low-level method can be either QM or molecular mechanics (MM). Any computational method can be used in ONIOM without modification, and in most cases, properties that can be obtained with the individual methods can also be obtained when those methods are combined in ONIOM. But despite this, few excited-state calculations have so far appeared in the literature using the ONIOM method[9,10,12–18] and none of these have fully optimized a conical intersection geometry.

To assess the suitability of the ONIOM method for locating conical intersection geometries and to establish good method combinations, we optimized one of the conical intersections in the reaction network of vitamin D,[19,20] where the partitioning is as shown in Figure 1. Our first test of ONIOM here will be to compare the geometries obtained with different combinations of methods to the full Target calculation. We used the precursor of vitamin D—previtamin D (precalciferol)—to test the ONIOM method because it has been the subject of many previous spectroscopic[21–23] and theoretical[24,25] studies, due to its biological and synthetic importance.

In addition to geometries, the second test of ONIOM here is the energy difference between an S_1/S_0 conical intersection and a nearby S_1 minimum: the cZt rotamer of previtamin D, which on the ground state exists in thermal equilibrium with a cZc rotamer as shown in Figure 2.

Our Target optimized S_1 minimum and the associated conical intersection geometry for previtamin D are shown in Figure 3, where the high-level region is highlighted.

We compared Target and model-only calculations—both using CASSCF/4-31G alone—with various ONIOM method combinations. CASSCF/4-31G was used as the ONIOM high level in each case (to match the Target), with low-level methods including MM (UFF), semiempirical (AM1), and ab initio QM methods (for both ground and excited states). In the next section, we discuss the use of ONIOM for excited-state geometry optimizations and crossing searches in more detail, before presenting and discussing the results for previtamin D, and evaluating the performance of the different method combinations. In evaluating the ONIOM calculations, we balance the accuracy of the geometries and energy differences obtained against the time the calculations took.

This work is primarily a proof-of-concept study: we aim to understand the behavior and technical aspects of the proposed method and the physical aspects of any approximations used. To do this in detail we focus on a single example (Figure 3) at

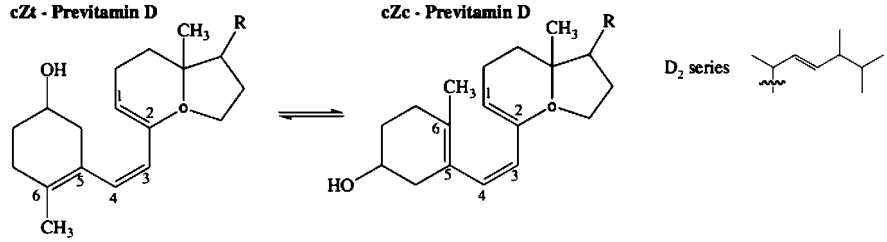

Figure 2. Thermal equilibrium mixture of the mono-s-trans (cZt) and all-s-cis (cZc) rotamers of previtamin D; the alkyl R group of the synthetic form (D_2 series) used here is shown. The carbon atoms of the hexatriene model system are labeled as in Figure 1 (and ref 24).

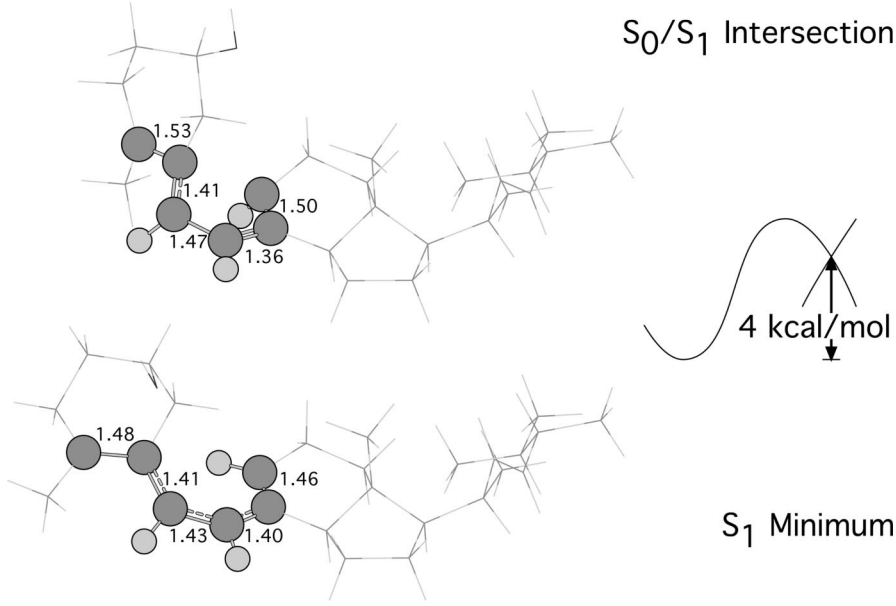

Figure 3. Target (CASSCF/4-31G) geometries (distances in angstroms) and relative energy on S_1 of the previtamin D structures studied here. The high-level hexatriene region is highlighted as a ball-and-bond structure.

a target level of theory (CASSCF/4-31G) that has a small but computationally manageable basis set; not aiming for absolute accuracy.

Computational Methods

The ONIOM energy for a two-layer system (two levels of theory) is written in the form of an extrapolation (eq 1). The real system contains all of the atoms, from both the high-level and low-level regions; the model system contains only the atoms that belong to the high-level region and the link hydrogen atoms that are used to saturate the dangling bonds that result from covalent interactions between the regions (Figure 1). The real system is only calculated with the low-level method, whereas the model system is calculated with both the high- and low-level methods. Particularly for the present work, it is important to realize that the terms $(E_{\text{real}}^{\text{low}} - E_{\text{model}}^{\text{low}})$ in eq 1 describe both the contribution from the low-level region (the region treated only at the low level of theory) as well as the interaction between the high-level and low-level regions. In other words, the coupling between the two regions is always evaluated at the low computational level of theory.

Because all the terms in eq 1 involve chemically realistic systems (Figure 1), ONIOM can be used to combine QM with QM methods, as well as QM with MM methods. The positions of the necessary link atoms are defined in terms of the positions of the corresponding atoms in the real system. The potential energy surface is therefore well defined, and any conventional method for the investigation of potential surfaces (e.g., gradient-driven optimization, IRC,...) can be used with ONIOM as well. Equation 1 can be generalized for any number of layers, where each additional layer introduces two additional energy calculations, but in the current work, we are only concerned with two-layer ONIOM calculations.

The ONIOM gradient can be written as

$$\begin{aligned}\mathbf{g}^{\text{ONIOM}} = \frac{\partial E^{\text{ONIOM}}}{\partial \mathbf{q}} &= \frac{\partial E_{\text{real}}^{\text{low}}}{\partial \mathbf{q}} + \frac{\partial E_{\text{model}}^{\text{high}}}{\partial \mathbf{q}^{\text{m}}}\mathbf{J} - \frac{\partial E_{\text{model}}^{\text{low}}}{\partial \mathbf{q}^{\text{m}}}\mathbf{J} \\ &= \frac{\partial E_{\text{real}}^{\text{low}}}{\partial \mathbf{q}} + \frac{\partial E_{\text{model}}^{\text{high}}}{\partial \mathbf{q}} - \frac{\partial E_{\text{model}}^{\text{low}}}{\partial \mathbf{q}}\end{aligned} \tag{4}$$

The Jacobian $\mathbf{J}$ converts the coordinate system for the model system, $\mathbf{q}^{\text{m}}$, to the coordinate system for the real system, $\mathbf{q}$.

Most studies that employ ONIOM involve electronic ground states, but the method can describe excited states as well.[9,10] Clearly, the high-level method must be able to describe an excited state (such as CASSCF, as used in this study) and the excitation must be (approximately) localized in the model system. However, the choice for low-level method and electronic state is less clear. Assuming that the excitation is completely localized in the high-level region, one can argue for a ground-state low-level method, because the excitation is the same in $E_{\text{real}}^{\text{low}}$ and $E_{\text{model}}^{\text{low}}$ and therefore cancels from $(E_{\text{real}}^{\text{low}} - E_{\text{model}}^{\text{low}})$. However, in this case, the interaction between the high- and low-level regions would be based only on the ground-state electronic structure, which may or may not be correct, depending on the system and process. It therefore seems formally necessary to employ an excited-state method for the low level, when calculating excited states with ONIOM. The excited-state energy is denoted E^*, and the ground-state energy as E (we discuss ground and excited-state potentials, but these could in fact be any pair of excited-state potentials). The ONIOM excited-state energy is then written as

$$E^{*,\text{ONIOM}} = E_{\text{model}}^{*,\text{high}} + E_{\text{real}}^{*,\text{low}} - E_{\text{model}}^{*,\text{low}} \tag{5}$$

The excitation energy (at a particular molecular geometry) is expressed as

$$\begin{aligned}\Delta E^{\text{ONIOM}} &= E^{*,\text{ONIOM}} - E^{\text{ONIOM}} \\ &= \left(E_{\text{model}}^{*,\text{high}} + E_{\text{real}}^{*,\text{low}} - E_{\text{model}}^{*,\text{low}}\right) - \left(E_{\text{model}}^{\text{high}} + E_{\text{real}}^{\text{low}} - E_{\text{model}}^{\text{low}}\right) \\ &= \left(E_{\text{model}}^{*,\text{high}} - E_{\text{model}}^{\text{high}}\right) + \left(E_{\text{real}}^{*,\text{low}} - E_{\text{real}}^{\text{low}}\right) - \left(E_{\text{model}}^{*,\text{low}} - E_{\text{model}}^{\text{low}}\right) \\ &= \Delta E_{\text{model}}^{\text{high}} + \Delta E_{\text{real}}^{\text{low}} - \Delta E_{\text{model}}^{\text{low}}\end{aligned} \tag{6}$$

As mentioned above, in some cases we can assume (or approximate) that the excitation is localized in the model region and therefore that the interaction between regions does not depend on the state. In this case $(E_{\text{real}}^{*,\text{low}} - E_{\text{model}}^{*,\text{low}}) \approx (E_{\text{real}}^{\text{low}} - E_{\text{model}}^{\text{low}})$, and we can replace the low-level excited-state calculations in eqs 5 and 6 with ground-state calculations. In the resulting equations we indicate this substitution with the constrained low-level state (CLS) label:

$$E^{*,\text{ONIOM}} \approx E^{*,\text{ONIOM-CLS}} = E_{\text{model}}^{*,\text{high}} + E_{\text{real}}^{\text{low}} - E_{\text{model}}^{\text{low}} \tag{7}$$

and hence,

$$\begin{aligned}\Delta E^{\text{ONIOM-CLS}} &= E^{*,\text{ONIOM-CLS}} - E^{\text{ONIOM}} \\ &= \left(E_{\text{model}}^{*,\text{high}} + E_{\text{real}}^{\text{low}} - E_{\text{model}}^{\text{low}}\right) - \left(E_{\text{model}}^{\text{high}} + E_{\text{real}}^{\text{low}} - E_{\text{model}}^{\text{low}}\right) \\ &= E_{\text{model}}^{*,\text{high}} - E_{\text{model}}^{\text{high}} \\ &= \Delta E_{\text{model}}^{\text{high}}\end{aligned} \tag{8}$$

This is an attractive approximation, because ground-state-only methods can be used in the low level (e.g., molecular mechanics), reducing the complexity and the computational time and giving us a far greater choice of low-level methods.

Since $(E_{\text{real}}^{*,\text{low}} - E_{\text{model}}^{*,\text{low}}) \approx (E_{\text{real}}^{\text{low}} - E_{\text{model}}^{\text{low}})$, we could invert the above approximation and constrain the low level to be the excited state, which we indicate with the CLS* label. In this case, the excited-state energy is equal to that from eq 5:

$$E^{*,\text{ONIOM}} = E^{*,\text{ONIOM-CLS*}} = E_{\text{model}}^{*,\text{high}} + E_{\text{real}}^{*,\text{low}} - E_{\text{model}}^{*,\text{low}} \tag{9}$$

However, the ground-state ONIOM energy is written as

$$E^{\text{ONIOM}} \approx E^{\text{ONIOM-CLS*}} = E_{\text{model}}^{\text{high}} + E_{\text{real}}^{*,\text{low}} - E_{\text{model}}^{*,\text{low}} \tag{10}$$

(with excited-state low-level terms) and

$$\begin{aligned}\Delta E^{\text{ONIOM-CLS*}} &= E^{*,\text{ONIOM-CLS}} - E^{\text{ONIOM-CLS*}} \\ &= \left(E_{\text{model}}^{*,\text{high}} + E_{\text{real}}^{*,\text{low}} - E_{\text{model}}^{*,\text{low}}\right) - \left(E_{\text{model}}^{\text{high}} + E_{\text{real}}^{*,\text{low}} - E_{\text{model}}^{*,\text{low}}\right) \\ &= E_{\text{model}}^{*,\text{high}} - E_{\text{model}}^{\text{high}} \\ &= \Delta E_{\text{model}}^{\text{high}}\end{aligned} \tag{11}$$

The resulting energy difference $\Delta E^{\text{ONIOM-CLS*}}$ is the same as $\Delta E^{\text{ONIOM-CLS}}$ from eq 8 above, although the ONIOM potential energy surfaces will not be the same, and, e.g., a stationary point for one approximation need not be a stationary point for the other. In fact, this CLS* approximation is not as attractive as the CLS approximation, because using an excited state for the low level increases the complexity of the calculation and the computational time and gives us fewer choices of low-level

method. Consequently, we focus on the CLS approximation in the results presented in the next section.

We now turn our attention to the location of surface crossings, or conical intersections, with ONIOM. A conical intersection is a structural bottleneck, through which ultrafast radiationless decay is possible between excited- and ground-state potential energy surfaces.[26–29] The intersection hyperline is $(N-2)$ dimensional, where N is the number of nuclear degrees of freedom. The plane that lifts the degeneracy is formed by the gradient difference ($\mathbf{x}$) between the two states and the derivative coupling ($\mathbf{y}$); these vectors comprise the branching space.[30] The states are no longer degenerate when the geometry is distorted along these two linearly independent nuclear coordinates ($\mathbf{x}$) and ($\mathbf{y}$):

$$\mathbf{x} = \frac{\partial(E - E^*)}{\partial \mathbf{q}} \tag{12}$$

$$\mathbf{y} = \left\langle \mathbf{C}^t \left(\frac{\partial \mathbf{H}}{\partial \mathbf{q}} \right) \mathbf{C}^* \right\rangle \tag{13}$$

When the energy is plotted in the branching space, the potential energy surfaces form a double-cone structure, i.e., a reaction funnel, through which multiple ground-state products can be formed, depending on the shape of the crossing and the reaction pathways that can be accessed from it.

Both branching space vectors can be calculated with CASSCF methods using state-averaged orbitals[31] as documented previously.[32,33] Standard geometry optimization methods can locate critical points[34] along the $(N-2)$ dimensional hyperline using a modified gradient:[35]

$$\tilde{\mathbf{g}} = 2(E^* - E)\frac{\mathbf{x}}{|\mathbf{x}|} + P\frac{\partial E^*}{\partial \mathbf{q}} \tag{14}$$

The first term on the rhs of eq 14 takes the system to the intersection space, while the second term minimizes the energy within the hyperline. P projects the gradient of the excited state onto the orthogonal complement of the $\mathbf{x}$,$\mathbf{y}$ plane that lifts the degeneracy. This is the intersection space, which to first order preserves the degeneracy of the electronic states.

For ONIOM conical intersection searches, we assume that the excitation is localized in the model system and that the interaction between the regions is the same for ground state and excited states. As shown in eq 8 (for the CLS approximation), the energy difference between the states is then determined by the high-level calculation only. This implies that only the high-level calculation on the model system determines the degeneracy. (As shown in Figure 3, we evaluate ONIOM method combinations by comparing energies and geometries of an S_0/S_1 conical intersection and nearby S_1 minimum for previtamin D. For the S_1 minimum, CLS* is not an approximation beyond that intrinsic to ONIOM, since we use excited-state methods for the low level as well as the high level, and the energy and gradient are integrated from three excited-state subcalculations. However, for the conical intersection, both CLS and CLS* are approximations, in the sense that the gradient difference and derivative coupling vectors—which determine the projected S_1 gradient—are only determined here from the high-level model calculation.) The modified gradient for conical intersection searches for ONIOM can therefore be written as

$$\tilde{\mathbf{g}}^{\text{ONIOM-CLS}} = 2(E^{*,\text{high}}_{\text{model}} - E^{\text{high}}_{\text{model}})\frac{\mathbf{x}^{\text{high}}_{\text{model}}}{\left|\mathbf{x}^{\text{high}}_{\text{model}}\right|} + P'\frac{\partial E^{*,\text{ONIOM-CLS}}}{\partial \mathbf{q}} \tag{15}$$

where

$$\mathbf{x}^{\text{high}}_{\text{model}} = \frac{\partial(E^{\text{high}}_{\text{model}} - E^{*,\text{high}}_{\text{model}})}{\partial \mathbf{q}} = \frac{\partial(E^{\text{high}}_{\text{model}} - E^{*,\text{high}}_{\text{model}})}{\partial \mathbf{q}^{\text{m}}}\mathbf{J} \tag{16}$$

and P' is determined using $\mathbf{x}^{\text{high}}_{\text{model}}$ and $\mathbf{y}^{\text{high}}_{\text{model}}$ (with the configuration coefficients for the high-level calculation):

$$\mathbf{y}^{\text{high}}_{\text{model}} = \left\langle \mathbf{C}^t \left(\frac{\partial \mathbf{H}^{\text{high}}_{\text{model}}}{\partial \mathbf{q}} \right) \mathbf{C}^* \right\rangle = \left\langle \mathbf{C}^t \left(\frac{\partial \mathbf{H}^{\text{high}}_{\text{model}}}{\partial \mathbf{q}^{\text{m}}} \right) \mathbf{C}^* \right\rangle \mathbf{J} \tag{17}$$

Since the modified gradient $\tilde{\mathbf{g}}^{\text{ONIOM-CLS}}$ (eq 15) only depends on $\mathbf{x}$ and $\mathbf{y}$ from the high-level calculation on the model system (eqs 16 and 17), the additional computational cost of ONIOM will be no more than if we were studying the model system alone. (Note that P' is sparse, and the nonzero space is determined only by the size of the model system.)

The methods just described have been implemented in a development version of the Gaussian program.[36]

Finally, we comment on the levels of theory used. All of the high-level ONIOM, Target, and model-only calculations were computed using the CASSCF/4-31G level of theory. The active space chosen was the six electrons in six orbitals of the π-system of hexatriene; this has been justified in other studies,[24,37,38] where the modest 4-31G basis set was sufficient to describe the structures adequately. (The same active space was used for all CASSCF calculations: Target, ONIOM model system, and when the low-level method describing the ONIOM real system is also CASSCF, thereby excluding C═C in the −R group shown in Figure 2 from the active space.) We used state-averaged orbitals for the conical intersection and state-specific orbitals for the S_1 minimum. The nocpmcscf approximation was used for the crossing search: this is a small approximation for the orbitals and hence the gradient in the region of the degeneracy. Here, the extra effort to avoid this approximation is not required, as we are comparing ONIOM to a Target calculation run with the same approximation.

We tested a variety of methods as low-level method. The molecular mechanics method, UFF,[39] and the semiempirical method, AM1,[40] will clearly not provide an accurate electronic description but may perform adequately for the geometrical structures. To include a more accurate electronic description in the low level, we used the unrestricted and restricted open-shell Hartree−Fock methods (UHF and ROHF, respectively) but with the small Slater-type STO-3G basis set. Different spin multiplicities were used to emulate the open-shell character of the wave function at the conical intersection geometry, which has four unpaired (weakly coupled) electrons. To describe the S_1 minimum, we also tested using singlet and triplet states, because this was successful in a previous ONIOM study.[9] We did not compare results with different spin multiplicities since this would produce a discontinuous potential energy surface. These calculations were somewhat hampered by the need for the spin densities in the model and real calculations to be comparable, as discussed in more detail below. The use of CASSCF as the low-level method removes the spin state issue, and we used both the ground state, CAS(S_0), and the excited state, CAS(S_1). In the combinations with alternative multiplicities or CASSCF, the choice of state for the low level is (formally) clear for the S_1 minimum, but not clear for the surface crossing, because there both the ground and excited states need to be described.

As indicated above, we investigated using triplet and quintet ground states in the low level to mimic the singlet first excited state and the pairing of electrons at the conical intersection for previtamin D. For these systems, it appears that there are often multiple UHF solutions, which are very close in energy and differ in the way the unpaired electrons are distributed. In fact,

TABLE 1: Spin Densities on Carbon Centers (Numbering in Figure 1) in the Hexatriene Fragment from the ROHF and UHF Wave Functions (STO-3G Basis)[a]

		ROHF(T)	ROHF(Q)	UHF(S)	UHF(T)	UHF(Q)
S_1 min-real	C_1	0.84	0.90	−1.09	1.10	1.14
	C_2	0.01	0.13	0.91	−0.80	0.81
	C_3	0.11	0.08	−0.98	0.84	−0.74
	C_4	0.07	0.86	0.99	0.84	0.99
	C_5	0.02	0.94	−0.99	−0.85	1.02
	C_6	0.86	0.93	1.14	1.14	1.09
S_1 min-model	C_1	0.86	0.92	−1.13	1.14	1.18
	C_2	0.01	0.12	0.95	−0.83	0.85
	C_3	0.11	0.09	−0.99	0.86	−0.75
	C_4	0.08	0.87	1.00	0.86	1.00
	C_5	0.02	0.98	−1.03	−0.89	1.06
	C_6	0.91	0.99	1.20	1.20	1.16
CI-real	C_1	0.82	0.92	1.19	1.00	1.09
	C_2	0.02	0.08	−0.91	0.72	0.73
	C_3	0.03	0.04	0.90	−0.80	−0.75
	C_4	0.17	0.90	−1.06	1.11	1.07
	C_5	0.00	0.93	1.05	−1.02	0.99
	C_6	0.85	0.95	−1.16	1.18	1.13
CI-model	C_1	0.84	0.95	1.23	1.03	1.12
	C_2	0.02	0.08	−0.95	0.75	0.76
	C_3	0.03	0.04	0.91	−0.82	−0.77
	C_4	0.17	0.91	−1.06	1.11	1.08
	C_5	0.00	0.96	1.08	−1.04	1.02
	C_6	0.91	1.00	−1.24	1.25	1.20

[a] The (unsigned) density on the remaining atoms never exceeds 0.2.

the most stable UHF solution for the real system (which includes an unsaturated −R group, Figure 2) and the most stable solution for the model system occasionally correspond to different electron pairings. However, in order for the ONIOM extrapolation to be valid, we need qualitatively the same wave function for both of the subcalculations. Therefore, the wave functions we selected do not always correspond to the most stable solutions. However, we have used equivalent UHF solutions at the S_1 minimum and S_0/S_1 conical intersection geometries. In Table 1 we show the Mulliken spin densities of those wave functions, where the atom labeling is as in Figure 1. In most cases the pattern of spin densities is the same for the conical intersection and the S_1 minimum structures.

When we use ROHF triplets for the low level the unpaired electrons are localized on C_1 and C_6, whereas with the ROHF quintet wave functions the unpaired electrons are located on C_1, C_4, C_5, and C_6. For all of the UHF wave functions, we find densities close to +1 or −1 on all the carbon centers in the hexatriene fragment, and the singlet and triplet wave functions are strongly spin-contaminated.

Results and Discussion

S_1 Minimum Structure. With a good ONIOM method combination, the parameters in the high-level region should be similar to the Target values, whereas the parameters in the low-level region are expected to resemble those of a conventional low-level calculation. To assess the performance of a certain ONIOM method combination, it therefore only makes sense to compare the values in the high-level region to the Target data.

In Table 2 we show the geometrical parameters involving the carbon centers in the hexatriene fragment of previtamin D (Figures 1 and 3) for the Target, model-only, and ONIOM S_1 minima. It is immediately clear that the model-only structure does not represent the Target well: the bond lengths and angles are still quite similar, but the central dihedral angle $C_2-C_3-C_4-C_5$ differs by nearly 30°. This is clearly the result of interactions between C_1 and the cyclic substituent on C_5/C_6, as shown in Figure 1, which is not included in the model-only calculation.

In the ONIOM calculations the interaction between C_1 and the cyclic substituent on C_5/C_6 is included, and we see that with every method combination, the dihedral angles are improved with respect to the model-only data: the mean difference from the Target for each parameter set, reported in Table 2, is markedly worse for the model-only calculations. For most low-level methods, the bond lengths and angles are also reproduced well, and we only see some larger deviations from the Target in the dihedral angles. This is expected because the dihedral angles are easily deformed, especially $C_2-C_3-C_4-C_5$, which has a central bond that is closer to single in the excited state, as shown in Figure 3.

The ab initio methods in the low level perform generally better than AM1 and UFF, as shown in Table 2. RHF is the only exception and yields errors similar to UFF. Overall, all of the ONIOM combinations reproduce the Target well and appear to include the substituent effect of the low level at least qualitatively.

S_1-S_0 Energy Difference at the S_1 Minimum Geometry. For each ONIOM combination, we calculated the difference between the S_1 and S_0 energies at the minimum on the S_1 potential surface. The resulting values are shown in Table 3. As outlined in the Computational Methods section, we use an approximation whereby the energy difference between the two states is determined only by the high-level calculations on the model system:

$$\Delta E = E^{*,\mathrm{high}}_{\mathrm{model}} - E^{\mathrm{high}}_{\mathrm{model}} = E^{\mathrm{S_1,CAS/4\text{-}31G}}_{\mathrm{model}} - E^{\mathrm{S_0,CAS/4\text{-}31G}}_{\mathrm{model}} \quad (18)$$

Because the low-level method affects the geometry of the high-level region, and therefore of the model system, the ΔE values in Table 3 are different for each low-level method. The calculation of ΔE with ONIOM in this way introduces an error in two distinct ways. First, the low-level method affects the

TABLE 2: Bond Lengths, Angles, and Dihedral Angles of the S_1 Minimum Geometries Given in Angstroms and Degrees, Respectively[a]

		ONIOM low-level methods (STO-3G basis):										
	Target	model-only	CAS(S_0)	CAS(S_1)	RHF	ROHF(T)	ROHF(Q)	UHF(S)	UHF(T)	UHF(Q)	UFF	AM1
						Bond Lengths						
R(1,2)	1.46	1.47	1.45	1.46	1.47	1.46	1.47	1.46	1.46	1.46	1.46	1.48
		0.01	*−0.01*	*0.00*	*0.01*	*0.00*	*0.01*	*0.00*	*0.00*	*0.00*	*0.00*	*0.02*
R(2,3)	1.40	1.41	1.39	1.40	1.39	1.40	1.40	1.39	1.39	1.40	1.40	1.40
		0.01	*−0.01*	*0.00*	*−0.01*	*0.00*	*0.00*	*−0.01*	*−0.01*	*0.00*	*0.00*	*0.00*
R(3,4)	1.43	1.43	1.44	1.43	1.43	1.43	1.43	1.44	1.43	1.43	1.44	1.44
		0.00	*0.01*	*0.00*	*0.00*	*0.00*	*0.00*	*0.01*	*0.00*	*0.00*	*0.01*	*0.01*
R(4,5)	1.41	1.38	1.42	1.41	1.42	1.41	1.41	1.41	1.41	1.41	1.43	1.41
		−0.03	*0.01*	*0.00*	*0.01*	*0.00*	*0.00*	*0.00*	*0.00*	*0.00*	*0.02*	*0.00*
R(5,6)	1.48	1.45	1.48	1.48	1.49	1.48	1.48	1.48	1.48	1.48	1.48	1.50
		−0.03	*0.00*	*0.00*	*0.01*	*0.00*	*0.00*	*0.00*	*0.00*	*0.00*	*0.00*	*0.02*
mean diff		0.02	0.01	0.00	0.01	0.00	0.00	0.00	0.00	0.00	0.01	0.01
						Bond Angles						
A(1,2,3)	124.35	127.72	124.54	124.79	124.58	124.63	124.85	124.51	124.58	124.92	123.04	125.86
		3.37	*0.19*	*0.44*	*0.23*	*0.28*	*0.50*	*0.16*	*0.23*	*0.57*	*−1.31*	*1.51*
A(2,3,4)	130.92	129.73	131.20	131.19	131.82	131.38	131.14	131.05	131.24	130.96	129.30	130.97
		−1.19	*0.28*	*0.27*	*0.90*	*0.46*	*0.22*	*0.13*	*0.32*	*0.04*	*−1.62*	*0.05*
A(3,4,5)	131.30	128.79	131.72	131.53	132.65	131.94	131.47	131.46	131.72	131.09	131.88	131.78
		−2.51	*0.41*	*0.22*	*1.35*	*0.64*	*0.17*	*0.16*	*0.42*	*−0.21*	*0.58*	*0.48*
A(4,5,6)	121.05	123.10	120.61	121.07	119.69	120.80	121.51	120.88	120.79	121.59	121.66	121.06
		2.05	*−0.44*	*0.02*	*−1.36*	*−0.25*	*0.46*	*−0.17*	*−0.26*	*0.54*	*0.61*	*0.01*
mean diff		2.28	0.33	0.24	0.96	0.41	0.30	0.16	0.31	0.34	1.03	0.51
						Dihedral Angles						
D(1,2,3,4)	−10.53	−6.74	−9.91	−10.98	−11.59	−9.71	−10.90	−9.89	−9.99	−11.71	−13.56	−10.23
		3.79	*0.62*	*−0.45*	*−1.06*	*0.82*	*−0.37*	*−0.64*	*0.54*	*−1.18*	*−3.03*	*0.30*
D(2,3,4,5)	−36.75	−7.97	−35.97	−34.87	−29.04	−34.85	−34.30	−37.20	−36.06	−35.10	−38.54	−33.43
		28.78	*0.78*	*1.89*	*7.71*	*1.90*	*2.46*	*−0.45*	*0.69*	*1.65*	*−1.79*	*3.32*
D(3,4,5,6)	175.49	177.94	174.73	175.40	176.55	175.75	176.92	175.44	175.49	177.16	172.45	176.14
		2.45	*−0.76*	*−0.09*	*1.06*	*0.26*	*1.43*	*−0.05*	*0.20*	*1.67*	*−3.04*	*0.65*
mean diff		11.67	0.72	0.81	3.28	0.99	4.26	0.38	0.48	1.50	2.62	1.42

[a] The atom numbering is given in Figure 1. The difference from the Target calculations is given below each measurement (in italic), and the mean unsigned difference is calculated for each parameter.

TABLE 3: S_1-S_0 Energy Differences (ΔE) at the S_1 Minimum Geometries (kcal·mol^{-1}) and the Dihedral Angle ($\angle$) Describing the C_6-Methyl Orientation (Degrees)[a]

	low-level method[b]	ΔE	$\Delta\Delta E$	$\Delta\Delta E'$	$\angle$(4,5,6,Me)	$\Delta\angle$(4,5,6,Me)
ONIOM-CLS	CAS(S_0)	64.30	−1.54	−5.00	35.6	29.9
	RHF	57.27	−8.57	−12.02	53.8	48.1
	ROHF(T)	65.43	−0.41	−3.87	21.6	15.9
	ROHF(Q)	66.32	0.48	−2.97	15.2	9.5
	UHF(S)	66.53	0.69	−2.77	22.8	17.1
	UHF(T)	66.06	0.22	−3.24	22.7	17.0
	UHF(Q)	66.84	1.00	−2.46	15.2	9.5
	UFF	59.77	−6.07	−9.52	43.4	37.7
	AM1	64.86	−0.98	−4.43	25.6	19.9
ONIOM-CLS*	CAS(S_1)	67.53	1.69	−1.76	17.1	11.4
	CAS(S_1)/4-31G	69.30	3.46	0	5.7	0
	model-only	68.76	2.92	−0.54	5.5	−0.2
	Target	65.84	0	−3.46	5.7	0

[a] $\Delta\Delta E$ and $\Delta\angle$ are the errors with respect to the Target results, and $\Delta\Delta E'$ is the error with respect to the low-level method CAS(S_1)/4-31G. [b] STO-3G basis unless indicated otherwise.

geometry of the model system, which may then not be the same as in the Target. Second, the low level only describes a specific electronic state, which effectively means that we force the difference in states to be localized in the high-level region. This is not necessarily a valid approximation. Although the low-lying states can be represented by the π-electronic system, the interaction with the electronic structure of the remainder of the system may still be significant. In the following paragraphs we will investigate both effects and relate these to the results in Table 3.

We first investigate the forced localization of the excitation process and calculate ΔE according to

$$\Delta E = \text{ONIOM(CAS(S}_1\text{)/4-31G : CAS(S}_1\text{)/4-31G)} - \text{ONIOM(CAS(S}_0\text{)/4-31G : CAS(S}_1\text{)/4-31G)} \quad (19)$$

This corresponds to the CAS(S_1)/4-31G entry in Table 3. The high level and low level of theory are identical, but we do use the CLS* approximation. The first term in eq 19, which describes the S_1 energy, is the same as the Target, and the

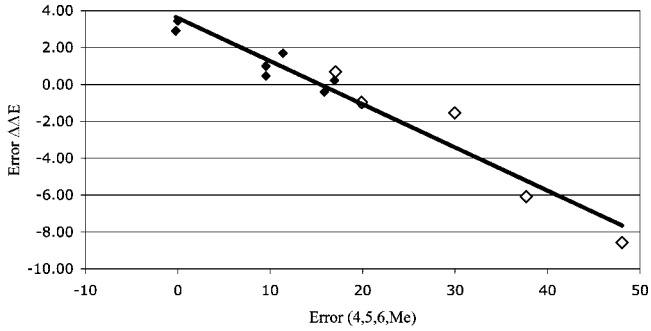

Figure 4. Error in the dihedral angle D(4,5,6,Me) (Table 3, degrees), relative to the Target, plotted against the error in the S_1-S_0 energy difference (Table 3, kcal·mol^{-1}), relative to the Target. Low-level methods that are formally ground state are plotted with open diamonds.

geometry for the S_1 minimum will therefore be identical to the Target as well. ΔE, on the other hand, is not identical to ΔE^{Target} ($= \Delta E^{\text{high}}_{\text{real}}$), since the low-level contribution in the second term is calculated for the excited state. In Table 3, we see that this ONIOM combination overestimates ΔE by about 3 kcal·mol^{-1}. Because the geometry is the same as for the Target, the error results completely from the localized description of the excitation and not from the level of theory that is used as the low-level method. Since the remaining ONIOM combinations also use the localized description, we cannot expect them to perform better than this.

Most of the ONIOM descriptions are reasonably close to the Target, or better, the ONIOM low-level method CAS(S_1)/4-31G value, which indicates that all low-level methods adequately describe the effect of the low-level region on the geometry of the high-level region. It turns out that the remaining error is specifically related to the orientation of the methyl group connected to C_6, and in Figure 4 we show the correlation between this error and the dihedral angle that describes the out-of-plane orientation of the methyl group. The (linear) best fit intersects with the Y-axis at 3.5 kcal·mol^{-1}, which is very close to the error due to the localized description of the two states. The dependence on the methyl orientation may be caused by the different nature of the C_5-C_6 bond in the two states. The C_5-C_6 bond is near-single (~1.48 Å) in the excited state and therefore easily deformed and sensitive to the level of theory. In the ground state, however, the bond is formally double, and even small deformations can affect the energy significantly. Furthermore, we can see that the largest errors occur with low-level methods that describe the ground state: CAS(S_0), RHF, UHF(S), UFF, and AM1. This is as expected, since the Target geometry is obtained for the S_1 state.

We would expect the ONIOM results to become closer to the Target and low-level CAS(S_1)/4-31G values by enlarging the high-level region to include the methyl group, and perhaps the second carbon center attached to C_6. We must keep in mind, however, that the errors in ΔE show up because the energy on the S_0 state does not correspond to an optimized structure on that surface. Since the primary goal of the current work is to investigate the relationship between the S_1 minimum and nearby S_1/S_0 conical intersection, which both are critical points, we decided not to investigate this further but to continue using the original partitioning into the high- and low-level regions (Figure 1).

S_1/S_0 Conical Intersection Structure. As for the S_1 minimum structure, we can only directly compare the ONIOM values of the high-level region with the Target calculation. The geometrical parameters of the corresponding carbon centers in the hexatriene fragment for the Target, model-only, and ONIOM conical intersection are shown in Table 4. The model-only structure represents the Target geometry better in this case than for the S_1 minimum. However, it is still markedly worse than all of the ONIOM calculations, especially for the ∠(4,5,6) angle and all the dihedral angles, particularly the final angle on ∠(3,4,5,6) which differs by nearly 10°. As was the case for the S_1 minimum geometry, the absence of the cyclic substituent means the model-only geometry is not capable of correctly describing the Target geometry. Most of the method combinations reproduce the Target results very well and are slightly better than the S_1 minimum geometries, presumably because the open-shell low-level methods emulate the electronic structure of the conical intersection better than that of the S_1 minimum. RHF and UFF perform the worst again, followed by AM1. The majority of the ab initio methods perform well: both CAS and quintet states of the Hartree−Fock calculations give small deviations from the Target values for all parameters. However, the methods which produce the best results are the triplet UHF and ROHF and the singlet UHF.

S_1 Minimum − Conical Intersection Energy Difference. In Table 5 we show the energy difference between the conical intersection (CI) and S_1 minimum points on the potential surface, calculated at the Target, model-only, and various ONIOM levels of theory. The first observation we make is that most of the ONIOM methods with QM methods in the low level yield results that are close or reasonably close to the Target value. UFF in the low level yields a significantly larger error ($\Delta\Delta E$) and a crossing below the minimum, whereas AM1 in the low level gives a small error, but with a sign opposite to that of all of the other methods, i.e., the energy difference on S_1 is larger than for the Target. Second, we find that there is no longer a correlation between the error and the methyl orientation. As outlined above, this is probably the result of both energies now being calculated at critical points on the same potential energy surface.

In the analysis of the S_1-S_0 energy difference at the S_1 minimum geometry, we separated the error resulting from the forced localization of the excitation and the error resulting from the use of a less accurate computational method in the low-level layer. This is not possible in the analysis of the CI−S_1 energy difference, because for the CI, ONIOM(CAS/4-31G:CAS/4-31G) is no longer equivalent to the Target CAS/4-31G calculation, as it was for the S_1 minimum. This is due to the fact that for the CI, the result depends directly on the difference between the S_1 and S_0 potential surfaces, which is not the case for the S_1 minimum structure. It is therefore harder to understand the errors in Table 5 than the errors in Table 3.

Still, the error formally results from both the forced localization and the use of a low-level method. In Table 3 we saw that the S_1-S_0 energy difference is overestimated due to the localization of the excitation. Since the CI involves both the ground state and the excited state, we can assume that its energy is again overestimated due to the forced localization, but overestimated less than the S_1 minimum energy, since the latter involves only the excited state. Overestimation of both energies—but less for the CI—should reduce the energy difference between the CI and S_1 minimum (see Figure 3). This is exactly what we observe in Table 5: all of the QM methods in the low level underestimate ΔE. However, we must keep in mind that the forced localization affects both the CI and S_1 minimum energies, and to some extend cancelation of errors will take place. Since it is hard to estimate the magnitude of

TABLE 4: Bond Lengths, Angles, and Dihedral Angles of the Conical Intersection Geometries Given in Angstroms and Degrees, Respectively[a]

		ONIOM low-level methods (STO-3G basis):										
	Target	model-only	CAS(S_0)	CAS(S_1)	RHF	ROHF(T)	ROHF(Q)	UHF(S)	UHF(T)	UHF(Q)	UFF	AM1
						Bond Lengths						
R(1,2)	1.50	1.48	1.50	1.50	1.50	1.50	1.50	1.50	1.50	1.50	1.53	1.51
		−0.02	*0.00*	*0.00*	*0.00*	*0.00*	*0.00*	*0.00*	*0.00*	*0.00*	*0.03*	*0.01*
R(2,3)	1.36	1.36	1.35	1.35	1.35	1.35	1.36	1.35	1.35	1.35	1.35	1.36
		0.00	*−0.01*	*−0.01*	*−0.01*	*−0.01*	*0.00*	*−0.01*	*−0.01*	*−0.01*	*−0.01*	*0.00*
R(3,4)	1.47	1.46	1.47	1.47	1.48	1.47	1.47	1.47	1.47	1.47	1.47	1.47
		−0.01	*0.00*	*0.00*	*0.01*	*0.00*	*0.00*	*0.00*	*0.00*	*0.00*	*0.00*	*0.00*
R(4,5)	1.41	1.39	1.40	1.40	1.40	1.40	1.39	1.40	1.40	1.40	1.41	1.41
		−0.02	*−0.01*	*−0.01*	*−0.01*	*−0.01*	*−0.02*	*−0.01*	*−0.01*	*−0.01*	*0.00*	*0.00*
R(5,6)	1.53	1.52	1.56	1.55	1.55	1.55	1.55	1.54	1.55	1.55	1.56	1.55
		−0.01	*0.03*	*0.02*	*0.02*	*0.02*	*0.02*	*0.01*	*0.02*	*0.02*	*0.03*	*0.02*
mean diff		0.01	0.01	0.01	0.01	0.01	0.01	0.01	0.01	0.01	0.01	0.01
						Bond Angles						
A(1,2,3)	116.79	117.09	116.77	117.20	116.94	116.78	116.62	116.76	117.02	116.45	117.75	117.97
		0.30	*−0.02*	*0.41*	*0.15*	*−0.01*	*−0.17*	*−0.03*	*0.23*	*−0.34*	*0.96*	*1.18*
A(2,3,4)	114.17	113.91	113.66	113.95	114.07	114.14	113.89	114.18	113.95	113.69	114.05	114.44
		−0.26	*−0.51*	*−0.22*	*−0.10*	*−0.03*	*−0.28*	*0.01*	*−0.22*	*−0.48*	*−0.12*	*0.27*
A(3,4,5)	116.90	114.03	116.51	115.88	114.70	116.87	116.45	116.55	116.40	116.35	119.38	116.40
		−2.87	*−0.39*	*−1.02*	*−2.20*	*−0.03*	*−0.45*	*−0.35*	*−0.50*	*−0.55*	*2.48*	*−0.50*
A(4,5,6)	118.83	124.01	119.16	119.41	120.10	118.51	119.88	118.95	119.11	119.50	118.41	119.59
		5.18	*0.33*	*0.58*	*1.27*	*−0.32*	*1.05*	*0.12*	*0.28*	*0.67*	*−0.42*	*0.76*
mean diff		2.15	0.31	0.56	0.93	0.10	−0.49	0.13	0.31	0.51	1.00	0.68
						Dihedral Angles						
D(1,2,3,4)	−6.14	−10.89	−7.36	−4.77	−4.31	−5.90	−6.93	−6.82	−7.08	−7.43	−4.00	−6.79
		−4.75	*−1.22*	*1.37*	*1.83*	*0.24*	*−0.79*	*−0.68*	*−0.94*	*−1.29*	*2.14*	*−0.65*
D(2,3,4,5)	−30.47	−25.79	−29.88	−32.57	−33.97	−30.38	−29.31	−29.63	−30.38	−29.76	−29.18	−28.93
		4.68	*0.59*	*2.10*	*−3.50*	*0.09*	*1.16*	*0.84*	*0.09*	*0.71*	*1.29*	*1.54*
D(3,4,5,6)	149.48	158.71	147.19	149.73	145.78	147.38	151.78	148.40	148.69	151.20	143.52	145.01
		9.24	*−2.29*	*0.25*	*−3.70*	*−2.10*	*2.31*	*−1.08*	*−0.79*	*1.72*	*−5.96*	*−4.47*
mean diff		6.22	1.37	1.24	3.01	0.81	1.42	0.87	0.61	1.24	3.13	2.22

[a] The atom numbering is given in Figure 1. The difference from the Target calculations is given below each measurement (in italic), and the mean difference is calculated, irrespective of sign, for each parameter.

TABLE 5: CI−S_1 Energy Differences (ΔE, kcal·mol^{-1}) and the Errors with Respect to the Target Results ($\Delta\Delta E$, kcal·mol^{-1})

	low-level method	ΔE	$\Delta\Delta E$
ONIOM	CAS(S_0)	2.24	−1.85
	CAS(S_1)	2.94	−1.15
	RHF	2.17	−1.92
	ROHF(T)	3.59	−0.50
	ROHF(Q)	1.65	−2.44
	UHF(S)	0.42	−3.67
	UHF(T)	1.72	−2.37
	UHF(Q)	2.08	−2.01
	UFF	−3.75	−7.84
	AM1	5.63	1.54
	model-only	0.02	−4.08
	Target	4.09	0

the cancelation, we assume that the error cancels exactly. On the basis of the data in Table 5, we then conclude that ROHF(T) is the best low-level method. Of course, it is surprising that the CAS low-level methods perform worse than ROHF(T). This suggests that the effects of the forced localization are in fact not the same for the S_1 minimum and CI structures.

Timing. We now comment on the timing data for the Target and ONIOM calculations. This is in order to give an indication of the speedup of the various ONIOM combinations used, but it must be noted that this data is computer-specific, depending on the processor type, number of processors, memory available, disk, etc.

The model-only calculation takes about 1% of the time taken for the Target calculation, for a single energy + gradient computation. The crossing search takes somewhat longer than the S_1 minimization, because of state averaging and the additional calculation of the nonadiabatic coupling terms (eq 13). However, because we did not compute the CPMCSCF contribution[31] for the crossing minimization search, this scales approximately the same as the S_1 minimization; hence, we obtain approximately the same speedup in both cases.

The fastest ONIOM calculations are with the UFF and AM1 low-level methods. For this system (previtamin D), these low-level real calculations are so fast that they do not affect the overall computational time, which is therefore comparable to the time taken for the model-only calculation. The energies obtained for these low-level methods were the least reliable in this study, but as these calculations are as fast as the model-only calculations, yet include the substituent effect and are therefore closer to the Target, we suggest that they could be effectively employed for initial structural determinations.

The most reliable low-level methods for relative energies here were ROHF(T) and CASSCF. The ONIOM calculations using ROHF(T) took about 2% of the time for the Target calculation per energy + gradient step; for CASSCF, this rises to 10%.

Finally, improving the Target level of theory—for example, by increasing the size of the basis set and/or computing the CPMCSCF contribution—will almost certainly increase the time for the Target calculation more than the ONIOM calculation. Hence, the speedups for using ONIOM would improve on the values quoted above, with respect to a more accurate Target.

Conclusions

We have shown that the ONIOM method can be used to reliably optimize a conical intersection between the ground and first excited states of previtamin D. These calculations were up to 100 times faster with little loss of accuracy compared to a full non-ONIOM calculation. The most accurate method combination was CASSCF/4-31G//ROHF/STO-3G(Triplet); the bond lengths and angles in the hexatriene model region were calculated to within 0.02 Å and 0.7°, respectively, and the relative energy between the conical intersection and its nearest associated S_1 minimum to within 0.5 kcal·mol^{-1} of the Target. All the method combinations selected produced accurate geometries including the UFF molecular mechanics and AM1 semiempirical methods, suggesting a cheap and efficient way of optimizing initial geometries.

ONIOM calculations using CASSCF as the low-level method are also promising, with errors in the CI−S_1 energy difference of 1.85 (S_0) and 1.15 (S_1) kcal·mol^{-1}, respectively. It is surprising that ROHF performs better than CASSCF in this study, since ROHF is a single-determinant method. This suggests that the accuracy of ROHF in this case may be due to a cancelation of errors.

We identified a strong dependency of the energy difference between the ground state and first singlet excited state on the orientation of a methyl group close to the hexatriene fragment. Enlarging the model system would probably reduce this dependency. The success of the current work may be related to the particular system we studied. For polar systems, the calibration of the ONIOM partitioning and method combinations is probably more complicated.[41]

The most significant assumption we made in the current work is that we forced the excitation to be localized in the model system. We have some indication of the error that is introduced by this approximation, which is quite minor for previtamin D, but it is not clear if this is generally the case. We intend to make the ONIOM excited-state methods more general by developing methods that do not have this restriction.

Our view is that the significance of this work is twofold. First, the application of ONIOM allows for an assessment of the localization of the excited states, which provides fundamental insight into the physical processes involved. Second, ONIOM can reduce the computational cost of high-accuracy calculations significantly. This will facilitate the use of more realistic models in future studies of photochemical processes. Alternative methods for such studies involving surface crossings are available, including faster conventional (nonhybrid) methods (see, for example, refs 42–44); these could also be used as part of an ONIOM calculation.

Finally, we note that this is a proof of concept: the time savings are considerable, but since we have only looked at two points on an excited-state potential energy surface of one system, with a modest one-electron basis set, we need more work to establish that ONIOM in general is as promising as this study suggests.

Acknowledgment. This work was supported by EPSRC U.K., Grant Reference GR/R75236/02. We thank Dr. Ayako Furuhama for suggestions concerning the presentation of this paper.

References and Notes

(1) Manthe, U.; Koppel, H. *J. Chem. Phys.* **1990**, *93*, 1658–1669.

(2) Olivucci, M.; Ragazos, I. N.; Bernardi, F.; Robb, M. A. *J. Am. Chem. Soc.* **1993**, *115*, 3710–3721.

(3) Bearpark, M. J.; Ogliaro, F.; Vreven, T.; Boggio-Pasqua, M.; Frisch, M. J.; Larkin, S. M.; Morrison, M.; Robb, M. A. *J. Photochem. Photobiol., A* **2007**, *190*, 207–227.

(4) Dreuw, A. *ChemPhysChem* **2006**, *7*, 2259–2274.

(5) Humbel, S.; Sieber, S.; Morokuma, K. *J. Chem. Phys.* **1996**, *105*, 1959–1967.

(6) Svensson, M.; Humbel, S.; Froese, R. D. J.; Matsubara, T.; Sieber, S.; Morokuma, K. *J. Phys. Chem.* **1996**, *100*, 19357–19363.

(7) Dapprich, S.; Komaromi, I.; Byun, K. S.; Morokuma, K.; Frisch, M. J. *J. Mol. Struct. (THEOCHEM)* **1999**, *462*, 1–21.

(8) Vreven, T.; Byun, K. S.; Komaromi, I.; Dapprich, S.; Montgomery, J. A.; Morokuma, K.; Frisch, M. J. *J. Chem. Theory Comput.* **2006**, *2*, 815–826.

(9) Vreven, T.; Morokuma, K. *J. Chem. Phys.* **2000**, *113*, 2969–2975.

(10) Vreven, T.; Morokuma, K. *Theor. Chem. Acc.* **2003**, *109*, 125–132.

(11) Vreven, T.; Morokuma, K. In *Annual Reports in Computational Chemistry 2*; Spellmeyer, D. C., Ed.; Elsevier: Amsterdam, 2006; Vol. 2, pp 37−53.

(12) Blomgren, F.; Larsson, S. *J. Phys. Chem. B* **2005**, *109*, 9104–9110.

(13) Yamada, A.; Ishikura, T.; Yamato, T. *Proteins: Struct, Funct, Bioinf.* **2004**, *55*, 1063–1069.

(14) Gascon, J. A.; Batista, V. S. *Biophys. J.* **2004**, *87*, 2931–2941.

(15) Raynaud, C.; Poteau, R.; Maron, L.; Jolibois, F. *J. Mol. Struct. (THEOCHEM)* **2006**, *771*, 43–50.

(16) Casadesus, R.; Moreno, M.; Lluch, J. M. *J. Photochem. Photobiol., A* **2005**, *173*, 365–374.

(17) Zhang, R. B.; Ai, X. C.; Zhang, X. K.; Zhang, Q. Y. *J. Mol. Struct. (THEOCHEM)* **2004**, *680*, 21–27.

(18) Walch, S. P. *Chem. Phys. Lett.* **2003**, *374*, 501–505.

(19) Jacobs, H. J. C. *Pure Appl. Chem.* **1995**, *67*, 63–70.

(20) Jacobs, H. J. C.; Havinga, E. In *Advances in Photochemistry*; Pitts, J. N., Hammond, G. S., Gollnick, K., Grosjean, D., Eds.; Wiley: New York, 1979; Vol. 11, pp 305−373.

(21) Anderson, N. A.; Shiang, J. J.; Sension, R. J. *J. Phys. Chem. A* **1999**, *103*, 10730–10736.

(22) Dauben, W. G.; Zhou, B. L.; Lam, J. Y. L. *J. Org. Chem.* **1997**, *62*, 9005–9008.

(23) Fuss, W.; Lochbrunner, S. *J. Photochem. Photobiol., A* **1997**, *105*, 159–164.

(24) Bernardi, F.; Olivucci, M.; Ragazos, I. N.; Robb, M. A. *J. Am. Chem. Soc.* **1992**, *114*, 8211–8220.

(25) Dmitrenko, O.; Vivian, J. T.; Reischl, U.; Frederick, J. H. *J. Mol. Struct. (THEOCHEM)* **1999**, *467*, 195–210.

(26) Yarkony, D. R. *Rev. Mod. Phys.* **1996**, *68*, 985–1013.

(27) Sicilia, F.; Blancafort, L.; Bearpark, M. J.; Robb, M. A. *J. Phys. Chem. A* **2007**, *111*, 2182–2192.

(28) *Conical Intersections: Electronic Structure, Dynamics and Spectroscopy*; Domcke, W., Yarkony, D. R., Köppel, H., Eds.; World Scientific: Singapore, 2004.

(29) Bernardi, F.; Olivucci, M.; Robb, M. A. *Chem. Soc. Rev.* **1996**, *25*, 321–328.

(30) Atchity, G. J.; Xantheas, S. S.; Ruedenberg, K. *J. Chem. Phys.* **1991**, *95*, 1862–1876.

(31) Yamamoto, N.; Vreven, T.; Robb, M. A.; Frisch, M. J.; Schlegel, H. B. *Chem. Phys. Lett.* **1996**, *250*, 373–378.

(32) Manaa, M. R.; Yarkony, D. R. *J. Chem. Phys.* **1993**, *99*, 5251–5256.

(33) Yarkony, D. R. *J. Phys. Chem.* **1993**, *97*, 4407–4412.

(34) Sicilia, F.; Bearpark, M. J.; Blancafort, L.; Robb, M. A. *Theor. Chem. Acc.* **2007**, *118*, 241–251.

(35) Bearpark, M. J.; Robb, M. A.; Schlegel, H. B. *Chem. Phys. Lett.* **1994**, *223*, 269–274.

(36) Frisch, M. J.; Trucks, G. W.; Schlegel, H. B.; Scuseria, G. E.; Robb, M. A.; Cheeseman, J. R.; Montgomery, J. A.; Vreven, T.; Scalmani, G.; Kudin, K. N.; Iyengar, S. S.; Tomasi, J.; Barone, V.; Mennucci, B.; Cossi, M.; Rega, N.; Petersson, G. A.; Nakatsuji, H.; Hada, M.; Ehara, M.; Toyota, K.; Fukuda, R.; Hasegawa, J.; Ishida, M.; Nakajima, T.; Honda, Y.; Kitao, O.; Nakai, H.; Li, X.; Hratchian, H. P.; Peralta, J. E.; Izmaylov, A. F.; Brothers, E.; Staroverov, V.; Kobayashi, R.; Normand, J.; Burant, J. C.; Millam, J. M.; Klene, M.; Knox, J. E.; Cross, J. B.; Bakken, V.; Adamo, C.; Jaramillo, J.; Gomperts, R.; Stratmann, R. E.; Yazyev, O.; Austin, A. J.; Cammi, R.; Pomelli, C.; Ochterski, J. W.; Ayala, P. Y.; Morokuma, K.; Voth, G. A.; Salvador, P.; Dannenberg, J. J.; Zakrzewski, V. G.; Dapprich, S.; Daniels, A. D.; Strain, M. C.; Farkas, O.; Malick, D. K.; Rabuck, A. D.; Raghavachari, K.; Foresman, J. B.; Ortiz, J. V.; Cui, Q.; Baboul, A. G.; Clifford, S.; Cioslowski, J.; Stefanov, B. B.; Liu, G.; Liashenko, A.; Piskorz, P.; Komaromi, I.; Martin, R. L.; Fox, D. J.; Keith, T.; Al-Laham, M. A.; Peng, C. Y.; Nanayakkara, A.; Challacombe, M.; Chen, W.; Wong, M. W.; Pople, J. A. *Gaussian Development Version*, revision E.05; Gaussian, Inc.: Wallingford, CT, 2006.

(37) Olivucci, M.; Bernardi, F.; Celani, P.; Ragazos, I.; Robb, M. A. *J. Am. Chem. Soc.* **1994**, *116*, 1077–1085.

(38) Celani, P.; Ottani, S.; Olivucci, M.; Bernardi, F.; Robb, M. A. *J. Am. Chem. Soc.* **1994**, *116*, 10141–10151.

(39) Rappe, A. K.; Casewit, C. J.; Colwell, K. S.; Goddard, W. A.; Skiff, W. M. *J. Am. Chem. Soc.* **1992**, *114*, 10024–10035.

(40) Dewar, M. J. S.; Zoebisch, E. G.; Healy, E. F.; Stewart, J. J. P. *J. Am. Chem. Soc.* **1985**, *107*, 3902–3909.

(41) Wanko, M.; Hoffmann, M.; Frauenheim, T.; Elstner, M. *J. Comput.-Aided Mol. Des.* **2006**, *20*, 511–518.

(42) Keal, T. W.; Koslowski, A.; Thiel, W. *Theor. Chem. Acc.* **2007**, *118*, 837–844.

(43) Izzo, R.; Klessinger, M. *J. Comput. Chem.* **2000**, *21*, 52–62.

(44) Levine, B. G.; Ko, C.; Quenneville, J.; Martinez, T. J. *Mol. Phys.* **2006**, *104*, 1039–1051.

JP802204W